An efficient volume improving method by using a modified Allen-Cahn equation

Yibao Li[a,], Shouren Lan[b,], Xin Liu[c,d], Bingheng Lu[e,f,g], Lisheng Wang[b,**]

[a] *School of Mathematics and Statistics, Xi'an Jiaotong University, Xi'an 710049, China*
[b] *Department of Automation, Shanghai Jiaotong University, Shanghai, 200240, China*
[c] *School of Electrical and Information Engineering, Tianjin University, Tianjin 300072, China*
[d] *The Center for Machine Vision and Signal Analysis, University of Oulu, Finland*
[e] *Collaborative Innovation Center of High-End Manufacturing Equipment, Xi'an Jiaotong University, Xi'an 710049, China*
[f] *National Institue of Additive Manufacturing, Xi'an 710049, China*
[g] *School of Mechanical Engineering, Dongguan University of Technology, Dongguan 523808, China*

Abstract

Classifying and rendering volumes of structure are two essential goals of the visualization process. However, small holes or non-smooth patches in visualized volumes are usually induced by the loss of some voxels. Beginning with the classified volumes, we propose a modified Allen-Cahn equation, which has the motion of mean curvature, to recover lost voxels and to fill holes. We obtain the probability function, which indicates the probability of each voxel being a volume voxel. Usually, the obtained probability function is smooth due to the motion of the mean curvature flow. Therefore visualization quality of volumes can be significantly improved. Because of the unconditional stable operator splitting method, we can use a large time step size. Our proposed numerical scheme is fast and can

[*] Shouren Lan contributed equally to this work with Yibao Li, and is the co-first author for this paper.

[**] Corresponding author

Email addresses: `yibaoli@xjtu.edu.cn` (Yibao Li), `lswang@sjtu.edu.cn` (Lisheng Wang)

URL: `http://gr.xjtu.edu.cn/web/yibaoli` (Yibao Li)

be straightforwardly applied to GPU-accelerated DCT implementation that performs up to many times faster than CPU-only alternatives. Many experimental results have been performed to demonstrate the efficient of the proposed method.

Keywords: Volume rendering, Volume repairing, Allen-Cahn equation, Mean curvature flow

1. Introduction

Volume rendering is an important visualization technique for exploring and visualizing volume data. In this technique, the transfer function (TF) assigns different volumes (or volume voxels) with different opacities and assigns different structures with different colors. Then it can determine which structure is visible and estimate whether or not a structure can be well visualized [1].

However rendered volume by the TF exhibits two drawbacks. One is that small fragments, unexpected volume patches, or even other volumes are visualized together with volumes of interest. The reason is because that volumes of different structures with similar attribution will have the same region in the TF space [2]. The other drawback is that small holes (or gaps) appear on the visualized volume, because a slightly smaller region is selected from the TF. For example, different volumes are firstly separated from a volume data based on volume connectivity [3], and then are classified by segmenting the transfer function space into different regions [4] or into different components [5]. In these methods, sometimes volume defects are generated. In order to generate a high-quality volume, it is necessary to overcome these two mentioned drawbacks. To our knowledge, the first mentioned drawback has been studied recently in [3]. However, the volume repairing problem – refer to the problem to fill in small holes and improve rough patches of volume-rendered volumes, is rarely studied.

In this paper, we will develop an effective method to improve the volume rendering quality. The reason why small holes (or gaps) or rough patches appear on the visualized volumes is because that some volume voxels are assigned with much low opacities. However, most labeled volume voxels, which have been assigned with high opacities, are rightly determined from the volume data. Beginning with these labeled volume voxels, we try to recover the lost volume voxels and fill the holes. Whenever lost volume voxels are well recovered (refer to assign them with high opacities as well), volume defects will be repaired in the volume rendering. Based on this idea, the volume repairing problem in this paper is modeled as a constrained diffusion. Such diffusion is described by a modified Allen-Cahn equation (AC) which has the motion of mean curvature [6]. In the diffusion processing, the modified Allen-Cahn equation will adaptively adjust opacities of those voxels that are around labeled volume voxels. Finally, a probability function, which indicates the probability of each voxel being a volume voxel, is obtained. Usually, the obtained probability function is smooth without small holes due to the motion of the mean curvature flow (See Fig. 1). Our proposed method has several benefits. First, beginning with the labeled volume voxels by using the TF, our method is performed without depending on the TF. Therefore, volume repairing can be addressed without increasing the dimensionality of the TF. It allows us to incorporate our method into other processions or transfer functions, for example transfer function using L-H histograms [7] or curvature-based [8] transfer function. Secondly, our algorithm is simple to implement and is guaranteed to produce the good volume.

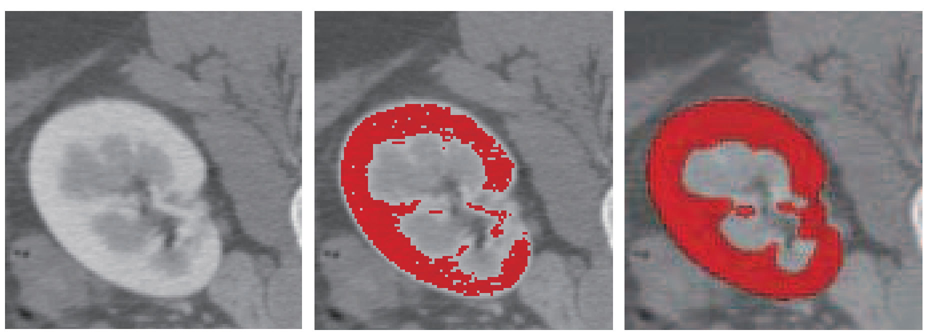

(a) **(b)** **(c)**

Figure 1: (a) Original 2D sectional slice. (b) Labeled volume by TF space (red color). (c) Repaired volume (red color). For the purposes of better visualization, the results are obtained in three dimensional space and are shown in a slice image.

The remainder of this paper is organized as follows: Section 2 discusses previous works related to our research. Section 3 introduces the proposed method to improve the visualized volume. Several experimental results are performed in Section 4. Conclusions and future work are presented in Section 5.

2. Related works

Volume reconstruction methods include the deformable volume method [9], the method for detecting and reconstructing implicit volume from volume data [10], the method based on marching cubes [11], the methods for reconstructing 3D volume from 3D cloud points [12] or range images [13], polygon-based isosurface-extraction repairing method [14], and volume-based isosurface-extraction repairing method [15] etc. While volume-based isosurface-extraction method and deformable volume methods can generate the closed volume. Other volume reconstruction methods usually generate the volume with small holes or fragments.

Volume-based isosurface-extraction repairing methods: Several isosurface-extraction volume repairing methods were studied. For example, beginning by constructing a signed distance function, Davis. et.al [15] applied a diffusion process to fill holes in complex surfaces. Their algorithm is simple to implement and is guaranteed to produce manifold non-interpenetrating surfaces. By combining information from the classifiers at the reconstruction stage, Lindholm. et.al [16] proposed an efficient approach to improve the classification of different material-

s. The volume-based methods generally patch the holes by first assigning signs to a set of 3D points (vertices of the polygonal volume) with a signed distance function. Then the point information in hole regions is completed in the volume representation. Finally, the repaired volume is given as an isosurface of the level set function. These volume-based methods can deal with topologically complex holes. However, they may miss some features of the original volume model when converting to and from a volume. Because the volume has been defined using the TF, it is not necessary to convert the volume for the initial processing. Therefore even with the volume-based method, these features can remain.

Volume repairing methods during volume rendering: Some researchers studied the improvement of volume rendering results of structures in a volume data. For example, defects of volume-rendered volumes were repaired by directly dilating all known volume voxels with a given radius [3]. However, this method usually incorrectly marks those voxels that are not volume voxels as volume voxels. In [17], some lost vessel structures in 3D MRA or CTA images were well enhanced by constructing a new vessel filter. However, this method cannot be applied to repair other structures. The method for filling-in holes by mathematical morphology was studied [18]. In this method, a filtered Euclidean skeleton is firstly utilized to represent thickness of the input object. After that, the authors transformed the closed thick object to the input one by using the dilation operator. However, this method cannot always obtain a smooth volume for topologically complex holes, because the operators of mathematical morphology cannot work well when the object is complex.

In this paper, we intend to repair volume defects by suitably diffusing labeled volume voxels in the volume data. Logically, some volume-based repairing methods based on the diffusion flow may be applied for such task. However, Allen–Cahn (AC) equation, which is a partial differential diffusing equation having the motion of mean curvature [6], has the following merits: (i) A fast and accurate hybrid numerical solver is available for the numerical computation of AC equation [19]. This makes the AC equation to be simple to implement and efficient to run on large data sets. (ii) The AC equation removes small local oscillations, which results in repairing the missing volume. (iii) The AC equation can deal with topologically complex holes. The AC equation has been applied in 2D image segmentation [20], 2D image inpainting [21], binary volume reconstruction [22], and multiple volume reconstruction [23]. Note that the modified AC equation has also been used in 2D image inpainting problem, which is the process of filling in missing parts of damaged images based on information from the surrounding areas [21]. In this paper, we use this equation in the different contexts and applications. To our knowledge, the presented approach is the first algorithm using the motion of mean curvature for the volume repairing in the volume data.

3. Methodology

In this section, we will introduce the modified Allen-Cahn equation to repair the volume. An unconditional stable resulting method will be developed. To well render the volume, volume voxels are assigned with suitable opacities.

3.1. A modified Allen-Cahn equation for volume repairing

Let $f(\mathbf{x})$ be a $3D$ image data in a domain $\Omega = (0, L_x) \times (0, L_y) \times (0, L_z)$, $\nabla f(\mathbf{x})$ be the gradient function of $f(\mathbf{x})$, where $\mathbf{x} = (x, y, z) \in \Omega$. In the volume rendering, a volume in $f(\mathbf{x})$ is determined by using the TF. By [3], the volume defect can be determined and denoted by a discrete function $\psi(\mathbf{x})$, where $\psi(\mathbf{x}) = 1$ if the voxel $\mathbf{x}$ is determined as a volume voxel, otherwise $\psi(\mathbf{x}) = 0$. As mentioned in above section, ψ contains lots of good volume voxels and few lost volume voxels. We want to obtain a new discrete function $\phi(\mathbf{x})$, which approaches to the given $\psi(\mathbf{x})$ and represents the volume without holes and rough patches.

As described in [24], volumes with zero mean curvature indicate that they are smooth and without holes. Meanwhile, the mean curvature of the lost volume will be much larger than zero. Therefore, the lost volume voxels can be detected by the mean curvature in the level set framework. Furthermore, keeping the mean curvature to be zero under a geometric evolution law will result in the removal of noises and repairing of the missing volume. Along this line, we assume the volume of the given volume data $\psi(\mathbf{x})$ can be moved under the mean curvature flow, in which the normal velocity of a moving hypersurface equals the negative mean curvature:

$$V_n = -\kappa,$$

where V_n is the normal velocity of geometric volume and κ is the mean curvature. Under the mean curvature flow, the volume in the repairing region will move faster than that in the non-repairing region because of its higher mean curvature value. Once the geometric volume is moved, the voxel near the volume will be filled by diffusing the information from the nearby region. While Eq. (1) is defined on the volume and will be difficultly performed as the volume moves. Allen-Cahn equation can be simply performed and has the motion of the mean curvature[6]:

$$\frac{\partial \phi(\mathbf{x},t)}{\partial t} = -\frac{F'(\phi(\mathbf{x},t))}{\varepsilon^2} + \Delta\phi(\mathbf{x},t) \tag{1}$$

Here $\phi(\mathbf{x},t)$ is also called as a phase-field function or probability distribution function, which is close to 1 and 0 for the volume's interior and exterior, respectively. ε is a constant and relates to the phase transition width. The function $F(\phi) = 0.25\phi^2(\phi-1)^2$ is a nonlinear potential function. To keep the voxel values outside of the repairing region be almost same as those in the original known volume, we should put a fitting term into the Allen-Cahn equation as:

$$\frac{\partial\phi(\mathbf{x},t)}{\partial t} = -\frac{F'(\phi(\mathbf{x},t))}{\varepsilon^2} + \Delta\phi(\mathbf{x},t) + \lambda(\mathbf{x})(\psi(\mathbf{x}) - \phi(\mathbf{x},t)),\ \mathbf{x}\in\Omega, \quad (2)$$

$$\phi(\mathbf{x},0) = \psi(\mathbf{x}), \quad (3)$$

$$\frac{\partial\phi(\mathbf{x},t)}{\partial \mathbf{n}} = 0, \quad \mathbf{x}\in\partial\Omega, \quad (4)$$

where

$$\lambda(\mathbf{x}) = \begin{cases} 0, & \text{if } \mathbf{x}\in\Omega_D, \\ \lambda_0, & \text{otherwise.} \end{cases} \quad (5)$$

Here λ_0 is a positive constant and Ω_D is the repairing region, which is simply defined as $\Omega_D = \{\psi(\mathbf{x})|\psi = 0\}$. The useful information has been labeled as $\psi = 1$ and less useful information is labeled as $\psi = 0$. We assume that ϕ satisfies Neumann volume conditions on $\partial\Omega$ as drawn in Eq. (4) and $\mathbf{n}$ is the outward normal vector. Eqs.(2)-(4) can be derived from a constrained gradient flow in the

L_2 space of the free energy functional:

$$\mathscr{E}(\phi)=\int_\Omega\left(\frac{F(\phi)}{\varepsilon^2}+\frac{|\nabla\phi|^2}{2}\right)d\mathbf{x}+\int_\Omega\frac{\lambda}{2}(\psi(\mathbf{x})-\phi)^2d\mathbf{x}.$$

The modified Allen-Cahn equation (Eq. (2)) keeps the total energy $\mathscr{E}(\phi)$ decrease with time:

$$\frac{d}{dt}\mathscr{E}(\phi)=\int_\Omega\Big(\frac{F'(\phi)}{\varepsilon^2}\phi_t+\nabla\phi\cdot\nabla\phi_t\Big)d\mathbf{x}-\lambda\int_\Omega(\psi-\phi)\phi_t d\mathbf{x} \tag{6}$$
$$=\int_\Omega\Big(-\frac{F'(\phi)}{\varepsilon^2}+\Delta\phi+\lambda(\psi-\phi)\Big)\phi_t d\mathbf{x}+\int_{\partial\Omega}\phi_t\varepsilon^2\mathbf{n}\cdot\nabla\phi ds=-\int_\Omega\phi_t^2d\mathbf{x}\leq 0.$$

It implies the solution of Eqs. (2)-(4) is uniqueness. Observing our modified Allen-Cahn equation, we can find that the voxel values in the repairing domain are obtained by curvature-driven diffusions due to the efficiency of Allen-Cahn equation. Because of the second term of Eq. (2), the voxel values outside of the repairing region will approach to those in the original volume data. Therefore the voxels can be well repaired. Furthermore, the final result ϕ can provide the probabilities of voxels belonging to the true volume (See Fig.(2)). For example, $\phi=0.5$ means that voxel has 50% probability belonging to the true volume.

Figure 3(a) shows the synthetic image with noises. Figure 3(b-e) are the results obtained by AC equation($\phi_t=-F'(\phi)/\varepsilon^2+\Delta\phi$), our proposed method

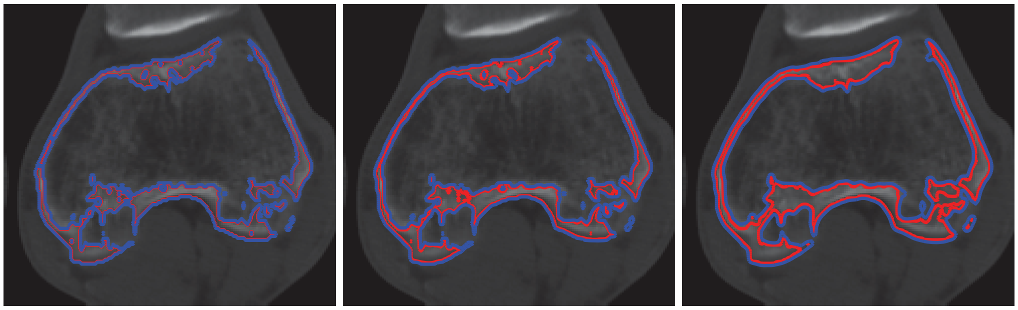

Figure 2: Evolution of the repairing volume method. From left to right, they are results at 0, 3, and 20 iterations. Red and blue lines denote the levels $\phi = 1$ and $\phi = 0.5$, respectively. Note that we perform the computation in the three dimensional domain.

($\phi_t = -F'(\phi)/\varepsilon^2 + \Delta\phi + \lambda(\psi - \phi)$), modified level set method ($\phi_t = |\nabla\phi|\nabla \cdot (\nabla\phi/|\nabla\phi|) + \lambda(\psi - \phi)$), and Laplacian smoothing method ($\phi_t = \Delta\phi + \lambda(\psi - \phi)$), respectively. With the classical AC equation, the noises are perfectly removed with missing the detail information of original image as shown in Fig. 3(b). The tips of the star move inward, while the gaps between the tips move outward, because the AC equation has the motion by mean curvature. On the other hand, our method smooths away noises while preserving the image detail as shown in Fig. 3(c). The modified level set method also works well as shown in Fig. 3(d). However in the level set framework, an explicit time integration scheme is a general choice for the mean curvature flow, which requires a small time step in order to ensure the numerical stability. In addition, the Laplacian smoothing method is simple and works well. But it leads to a over-smooth result compared to our proposed method.

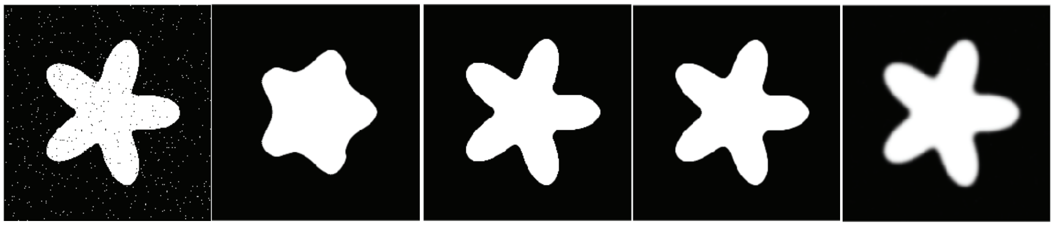

(a) (b) (c) (d) (e)

Figure 3: Results obtained by several different methods. (a)Synthetic image with noises. (b-e)Results obtained by AC equation($\phi_t = -F'(\phi)/\varepsilon^2 + \Delta\phi$), our proposed method ($\phi_t = -F'x(\phi)/\varepsilon^2 + \Delta\phi + \lambda(\psi - \phi)$), modified level set method ($\phi_t = |\nabla\phi|\nabla\cdot(\nabla\phi/|\nabla\phi|) + \lambda(\psi - \phi)$), and Laplacian smoothing method ($\phi_t = \Delta\phi + \lambda(\psi - \phi)$), respectively.

3.2. Opacity setting of the repaired volumes

In practice, some incorrectly voxels are partially reduced by assigning certain weights to their opacity values. xThe solution of Eqs.(2)-(4), $\phi(\mathbf{x})$, provides the probability of the voxel belonging to the true volume. Note that we regard the solution $\phi(\mathbf{x})$ as the steady state solution, if the relative error $\partial\phi(\mathbf{x},t)/\partial t$ is less than a tolerance tol. We determine the voxels with high probabilities such as $\phi(\mathbf{x}) > \alpha$ be the repaired volume voxels. Here $\alpha \in (0,1]$ is a constant. We will design the transfer function based on the obtained solution $\phi(\mathbf{x})$ and the given volume data $\psi(\mathbf{x})$. Every voxel in the volume is assigned with an opacity value by its probability value. Generally, higher the probability value of a voxel, larger the opacity of the voxel. However, some voxels, which are not volume voxels, may be assigned with high probabilities. Then we will modify their opacity values by assigning them with particular weights computed based on their gray values

$f(\mathbf{x})$. Usually, those voxels have similar gray values in their neighbor regions. If a recovered volume voxel has a gray value among its distribution, then it will be assigned with a large weight, otherwise it will be assigned with a small weight. Larger the distance, smaller the weight. In this paper, we use the following opacity setting:

$$Opa(\mathbf{x}) = \begin{cases} \mathbf{w}\phi(\mathbf{x}), \text{ if } \ \phi(\mathbf{x}) > \alpha, \\ 0, \qquad\quad \text{otherwise,} \end{cases} \tag{7}$$

where

$$\mathbf{w} = \begin{cases} 1, \text{ if } \ \psi(\mathbf{x}) = 1, \\ \beta, \text{ if } \ \psi(\mathbf{x}) = 0 \ \text{ and } \ \mathbf{x} \in \mathbf{K}_8, \\ \gamma, \text{ otherwise.} \end{cases} \tag{8}$$

Here $\beta \in (0,1)$, $\gamma \in (0,1)$, and $\beta > \gamma$. $\psi(\mathbf{x}) = 1$ implies that the voxel $\mathbf{x}$ is in the given volume region. $\mathbf{x} \in \mathbf{K}_8$ means the scalar value of 3D image at $\mathbf{x}$ satisfies $|f(\mathbf{x}) - f_{max}| \leq 8$ or $|f(\mathbf{x}) - f_{min}| \leq 8$. Here f_{max} and f_{min} are the maximum and minimum scalar values of 3D image, respectively. All through the paper, we set $\alpha = 0.3$, $\beta = 0.7$, and $\gamma = 0.3$. It implies that we only consider the voxel, whose property is larger than 0.3. If the considered voxel has been already labeled in the given volume, we will set $\mathbf{w} = 1$ and make the voxel be completely transparent. Otherwise, we will set $\mathbf{w} = \beta = 0.7$, if its gray value is much similar with its neighbor region in the 3D image. If the considered voxel has not been labeled in the given volume and its gray value is much different compared with its neighborhood in the 3D image, we will set $\mathbf{w} = \gamma = 0.3$ to make its volume with a low opacity. Note that α, β, and γ are chosen based on the experience of user. In summary, the flowchart of the framework for improving the visualized volume is drawn in Fig. 4.

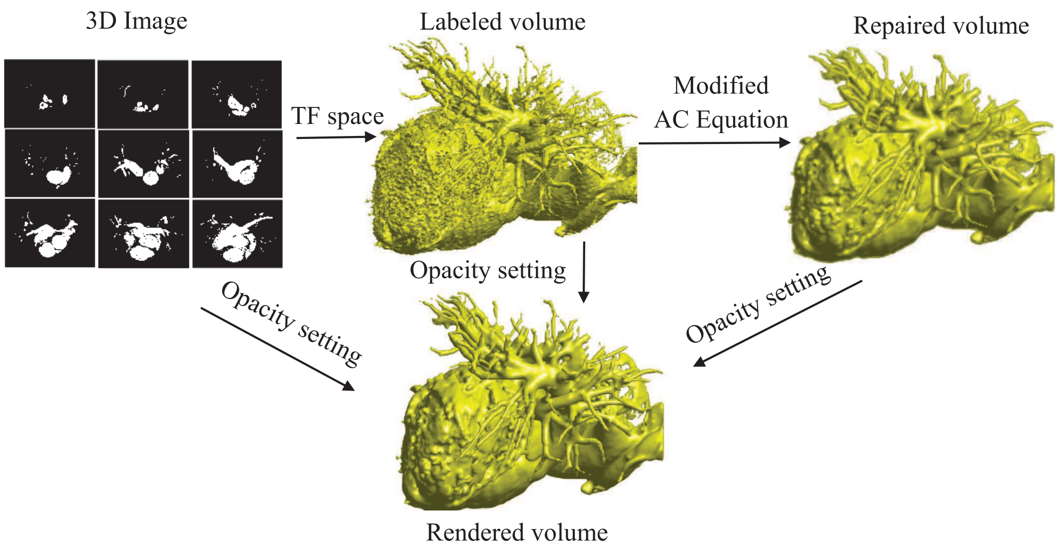

Figure 4: The flowchart of the framework for improving the visualized volume.

3.3. Numerical computation

Let $x_i = ih_x$, $y_j = jh_y$, $z_k = kh_z$, $1 \le i \le N_x$, $1 \le j \le N_y$, and $1 \le k \le N_z$, where N_x, N_y, and N_z are positive integers and h_x, h_y, h_z are the uniform mesh spaces. Let $\mathbf{x}_{ijk} = (x_i, y_j, z_k)$ and ϕ_{ijk}^n be an approximation of $\phi(\mathbf{x}_{ijk}, n\Delta t)$, where Δt is the time step. To obtain an unconditional stable scheme, we split the original problem (2) into a sequence of simpler problems by using the operator splitting-based hybrid numerical method:

$$\begin{cases} \frac{\partial}{\partial t}\phi_1(\mathbf{x},t) = \lambda(\mathbf{x})(\psi(\mathbf{x}) - \phi_1(\mathbf{x},t)), & (n-1)\Delta t < t \le n\Delta t, \\ \phi_1(\mathbf{x},(n-1)\Delta t) = \phi(\mathbf{x},(n-1)\Delta t), & \end{cases} \tag{9}$$

$$\begin{cases} \frac{\partial}{\partial t}\phi_2(\mathbf{x},t) = \Delta\phi_2(\mathbf{x},t), & (n-1)\Delta t < t \le n\Delta t, \\ \phi_2(\mathbf{x},(n-1)\Delta t) = \phi_1(\mathbf{x},n\Delta t), & \end{cases} \tag{10}$$

and

$$\begin{cases} \frac{\partial}{\partial t}\phi_3(\mathbf{x},t) = -\frac{F'(\phi_3)}{\varepsilon^2}, & (n-1)\Delta t < t \le n\Delta t, \\ \phi_3(\mathbf{x},(n-1)\Delta t) = \phi_2(\mathbf{x},n\Delta t). & \end{cases} \tag{11}$$

Here ϕ_1, ϕ_2, and ϕ_3 can represent the solutions for the subproblems (9), (10), and (11), respectively. Then the split solution at time $t = n\Delta t$ is defined as $\phi(\mathbf{x}, n\Delta t) = \phi_3(\mathbf{x}, n\Delta t)$. For a fixed $\mathbf{x}$, Eq. (9) is a separable ordinary differential equation, i.e., $\lambda dt + \frac{1}{\phi-\psi} d\phi = 0$. With the initial condition ϕ_{ijk}^n, we have the following solution after Δt:

$$\phi_{1,ijk}^{n+1} = e^{-\lambda\Delta t}\phi_{ijk}^n + (1-e^{-\lambda\Delta t})\psi_{ijk}. \tag{12}$$

Next, we solve Eq. (10) by applying an implicit method with ϕ_1^{n+1} and homogeneous Neumann volume condition, that is,

$$\frac{\phi_{2,ijk}^{n+1} - \phi_{1,ijk}^{n+1}}{\Delta t} = \Delta\phi_{2,ijk}^{n+1}. \tag{13}$$

The resulting discrete equations is solved by a fast solver such as fast discrete cosine transform. Then, for a fixed $\mathbf{x}$, Eq. (11) is a separable ordinary differential equation, i.e.,

$$0 = \frac{dt}{\varepsilon^2} + \frac{d\phi}{F'(\phi)} = \frac{dt}{\varepsilon^2} + \frac{-2d\phi}{\phi} + \frac{4d\phi}{\phi - 0.5} + \frac{2d\phi}{1-\phi}. \tag{14}$$

With the initial condition $\phi_{2,ijk}^{n+1}$, the solution can be obtained as

$$\phi_{ijk}^{n+1} = \phi_{3,ijk}^{n+1} = \frac{1}{2} + \frac{\phi_{2,ijk}^{n+1} - 0.5}{\sqrt{e^{\frac{-\Delta t}{2\varepsilon^2}} + (2\phi_{2,ijk}^{n+1} - 1)^2 (1 - e^{\frac{-\Delta t}{2\varepsilon^2}})}}. \tag{15}$$

$$\begin{tikzcd}[column sep=huge, row sep=huge]
\phi^n \arrow[r, dashed] \arrow[d, "\substack{\phi_t = \lambda(\psi - \phi) \\ \text{Analytical solution } \left(\text{Eq. (12)}\right)}"'] & \phi^{n+1} \\
\phi_1^{n+1} \arrow[r, "\substack{\phi_t = \Delta\phi \\ \text{Discrete cosine transform}}"'] & \phi_2^{n+1} \arrow[u, "\substack{\phi_t = F'(\phi)/\varepsilon^2 \\ \text{Analytical solution } \left(\text{Eq.(15)}\right)}"']
\end{tikzcd}$$

Figure 5: A hybrid numerical method for the original problem (2).

The proposed operator splitting algorithm is shown schematically in Fig. 5. The procedure of improving volume repairing is simple and summarized here. Beginning with the volume ψ from a 3D image using the TF method, we perform Eqs. (12)-(15), until $\|\phi^{n+1} - \phi^n\|_2^2 / \|\phi^n\|_2^2 < tol$. Then we set opacity by using Eqs. (7)-(8) and render the repaired volume. Our proposed numerical scheme has a merit that it can be straightforwardly applied to GPU-accelerated DCT implementation that performs up to many times faster than CPU-only alternatives.

3.4. Unconditional stability of our numerical method

In this section, we will prove the unconditional stability of our proposed scheme. For Eq. (12), since ϕ^n and ψ are assumed as in $[0,1]$, we get

$$0 \le \phi_1^{n+1} \le e^{-\lambda \Delta t} + (1 - e^{-\lambda \Delta t}) = 1. \tag{16}$$

Since Eq. (13) is a heat equation, its implicit numerical scheme is unconditionally stable and the inequality $\inf(\phi_1^{n+1}) \le \phi_2^{n+1} \le \sup(\phi_1^{n+1})$ is satisfied by the discrete minimum and maximum principles [25]. Therefore, $\phi_2^{n+1} \in [0,1]$ because $\phi_1^{n+1} \in [0,1]$. Secondly, for Eq. (15), we get

$$\phi^{n+1} = \begin{cases} 1 & \text{if} \quad \phi_2^{n+1} = 1, \\ \frac{1}{2} + \dfrac{1}{2\sqrt{1 + \left((2\phi_2^{n+1} - 1)^{-2} - 1\right) e^{\frac{-\Delta t}{2\varepsilon^2}}}} \le 1 & \text{if} \quad \phi_2^{n+1} \in (0.5,\ 1), \\ \frac{1}{2} & \text{if} \quad \phi_2^{n+1} = 0.5, \\ \frac{1}{2} - \dfrac{1}{2\sqrt{1 + \left((2\phi_2^{n+1} - 1)^{-2} - 1\right) e^{\frac{-\Delta t}{2\varepsilon^2}}}} \ge 0 & \text{if} \quad \phi_2^{n+1} \in (0,\ 0.5), \\ 0 & \text{if} \quad \phi_2^{n+1} = 0. \end{cases} \tag{17}$$

Thus if $\phi_2^{n+1} \in [0,1]$, then $\phi^{n+1} \in [0,1]$. Therefore our proposed scheme, Eqs. (12-15), is unconditionally stable for any time step, because any numerical solution ϕ

is bounded and is always in $[0,1]$.

4. Experimental results

In this section, we use the following parameters: $\Delta t = 0.5$, $h_x = h_y = 1$, $tol = 1e-4$, and $\lambda_0 = 5$. h_z is set according to the inter-slice spacing in CT images. ε is defined as $\varepsilon = \varepsilon_m = hm/[4\sqrt{2}\tanh^{-1}(0.9)]$ and $m = 12$ is chosen in this paper. We apply our method to improve the quality of volumes for several CT data sets. Figure 6 and Figure 7 show the repaired volumes by the proposed method. It can be observed that the original volume defects are well repaired.

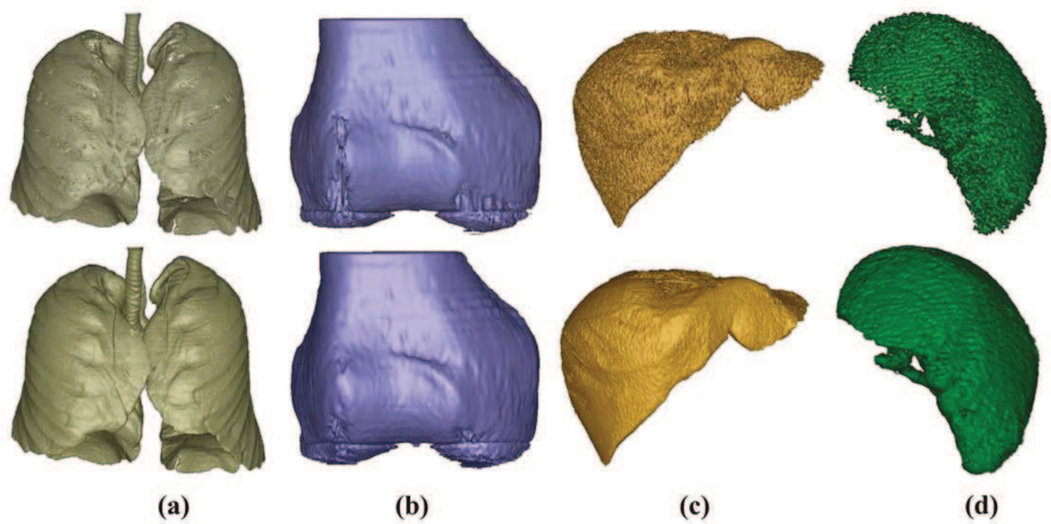

Figure 6: Repaired volumes by the proposed method. The first and second rows are the original and repaired volumes, respectively.

Table 1 provides the information of the iteration number and the CPU time. The CPU times (seconds) of our calculations, which are performed in *MATLAB*,

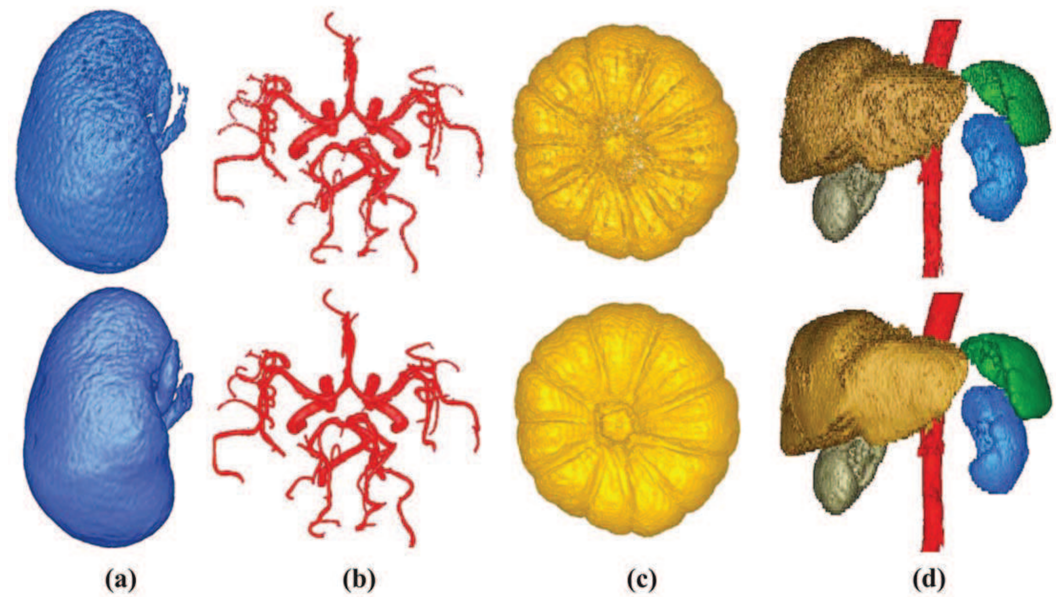

Figure 7: Repaired volumes by the proposed method. The first and second rows are the original and repaired volumes, respectively.

are measured on a desktop computer with 3.6 GHz with 16 G of RAM. As can be observed that the proposed method can achieve fast convergence after a few iterations, as expected from the unconditionally stable discrete scheme. Observing the elapsed CPU time, we can see that our method is fast, since our algorithm consists of two explicit evaluations of the closed-form solutions and one implicit heat equation solver. For the two linear equations, their computational complexities are $O(N)$, where N is the size of the mesh grid. For the heat equation solver, we apply a GPU-accelerated fast discrete cosine transform method with a computational complexity of $O(NlogN)$. Therefore our method is fast and simple.

Table 1: Performance of our proposed method.

Case	Mesh size	$h_x : h_y : h_z$	Iterations	CPU time (s)
Fig.6(a)	$112 \times 120 \times 104$	$1:1:1.5$	14	0.280
Fig.6(b)	$192 \times 192 \times 128$	$1:1:1.0$	20	1.516
Fig.6(c)	$256 \times 256 \times 80$	$1:1:2.5$	33	3.954
Fig.6(d)	$512 \times 512 \times 100$	$1:1:3.4$	26	8.614
Fig.7(a)	$448 \times 328 \times 272$	$1:1:1.5$	33	18.65
Fig.7(b)	$168 \times 152 \times 128$	$1:1:1.0$	15	0.740
Fig.7(c)	$312 \times 232 \times 168$	$1:1:1.5$	19	3.495
Fig.7(d)	$168 \times 152 \times 40$	$1:1:3.8$	18	0.312

4.1. Comparisons with related works and accuracy test

In [3], volume defects were repaired by directly dilating given volume voxels with a radius in 3D images. However, due to the dilation operation, the volumes repaired in [3] are usually thicker than the real volumes, as shown Fig. 8(b). Unlike the method in [3], the repaired volumes using our proposed method are in quality agreement with the real volumes, as illustrated in Fig. 8(a). Figure 8(c) and (d) are the two dimensional results of Fig. 8 (a) and (b), respectively. Here the original CT image is overlapped with the labeled volume. It implies that our proposed method is more appropriate for repairing volumes than one in [3].

Figure 9 shows the original volume over some CT slices of a kidney and repaired volume by using our proposed method. It can be seen that, the repaired volume without holes is in good agreement with the real volume in CT images.

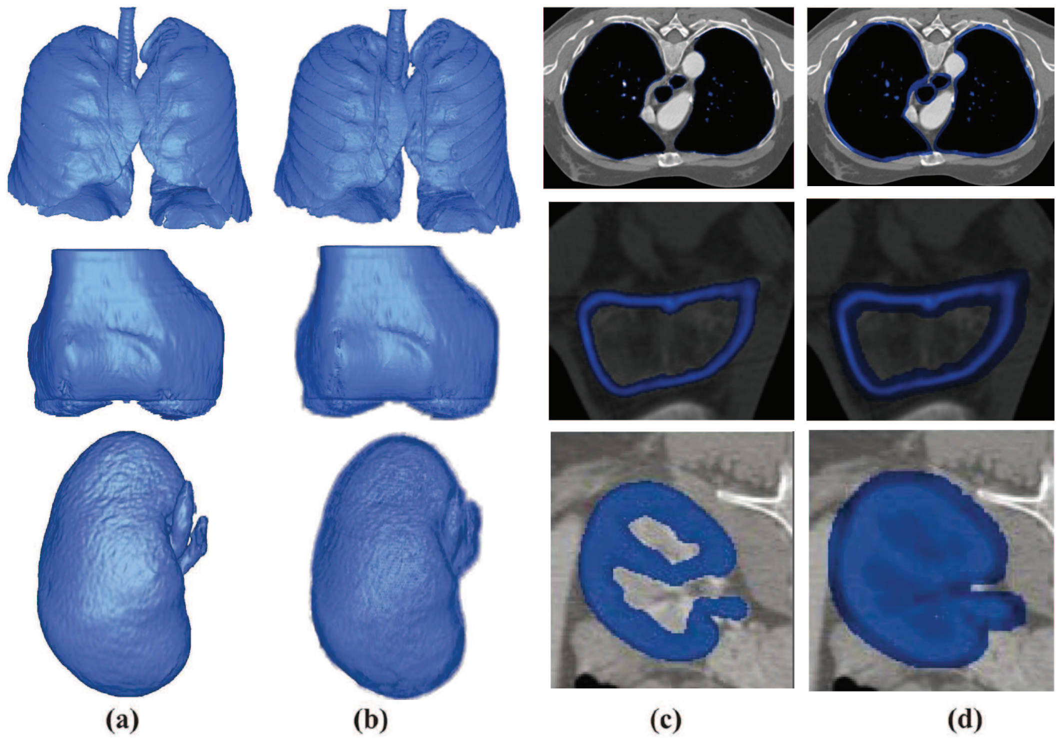

Figure 8: Comparison between our proposed model (a) and Lan et. al's model [3](b) in the CT slice. (c) and (d) are the two dimensional results of (a) and (b), respectively. Here the original CT image is overlapped with the marked voxel.

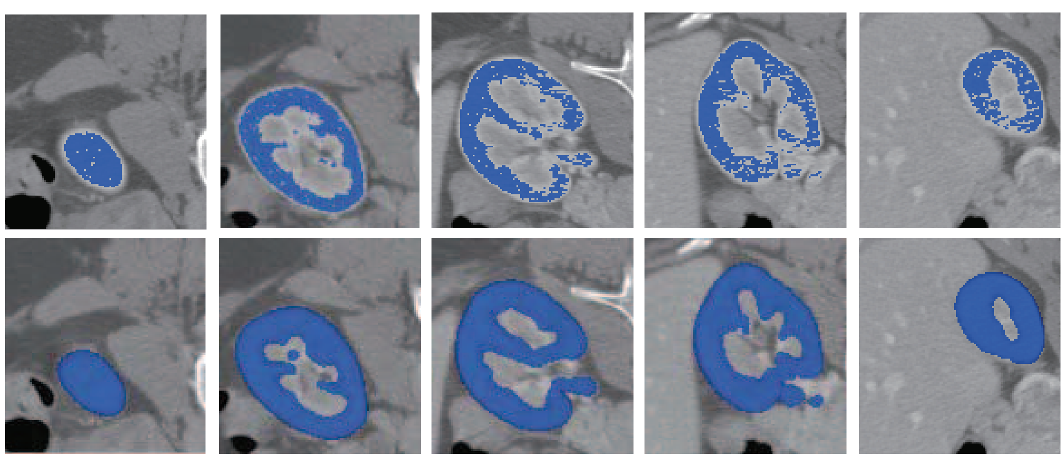

Figure 9: From top to bottom are 2D sectional slices with known volume and 2D sectional slices with repaired volume, respectively. From left to rights are the slices at 10, 30, 50, 70, and 90, respectively.

In Fig. 10, we compare the visualized results of volumes repaired by our proposed method with the ground-truth results (i.e., organs such as CT Liver, Aorta, Left Kidney, Right Kidney, and Spleen manually labeled from the CT image by experts). As can be seen that the agreement between the repaired volume and the ground-truth is obvious.

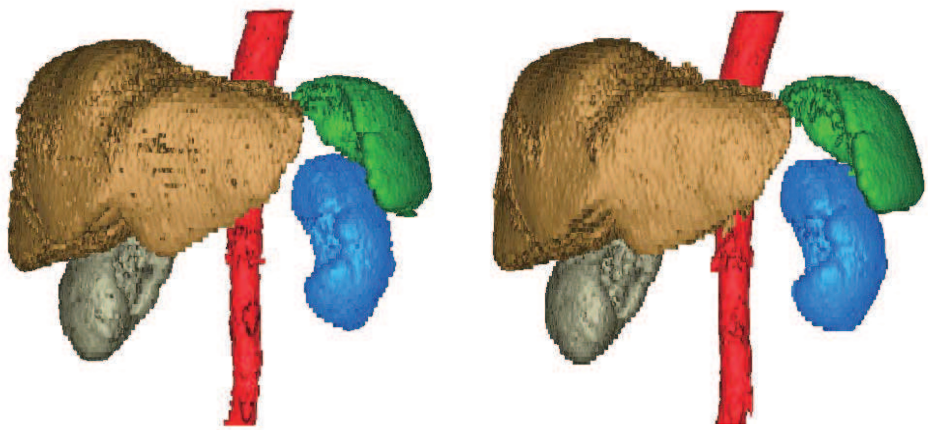

Figure 10: Comparison between ground-truth (left) and our proposed model (right).

We evaluate the quality of the volume based on the ground truth of multi-atlas of some abdominal CT images. To get an accurate evaluation of the proposed method, the criteria of Recall, Precision and DSC are employed. Precision is defined as the ratio of classified positive volumes to the total number classified volumes. Recall is defined as the ratio of the number of classified positive volumes to the total number of positive volumes in the ground-truth. DSC is dice coefficient. The definition of the performance measures are given below:

$$Recall = \frac{TP}{TP+FN}, \quad Precision = \frac{TP}{TP+FP}, \text{ and } DSC = \frac{2TP}{2TP+FP+FN}. \tag{18}$$

Where, TP (true positives) is the total number of organ voxels which are correctly classified, FN (false negatives) accounts for the number of organ volumes which are incorrectly classified, and FP (false positives) is the total number of those volumes that are incorrectly classified as organ volumes. Laplacian smoothing method can smooth a volume data and fill the holes by using the following governing equation: $\frac{\partial \phi(\mathbf{x},t)}{\partial t} = \Delta\phi(\mathbf{x},t) + \lambda(\mathbf{x})(\psi(\mathbf{x}) - \phi(\mathbf{x},t))$. Note that as $\varepsilon \to \infty$, our method will become the Laplacian smoothing method. To compare with the results obtained by using the previous method [3] and the Laplacian smoothing method, we put them together. Table 2 shows the accurate evaluations of the three mentioned methods. We can see that the Precision values of the three methods are qualitatively in good agreement with the theoretical values. Because the previous method [3] directly dilates all known volumes with a given radius as shown in Fig. 8(a) and (c), almost all correctly classified volumes can be marked. Hence, the number of incorrectly classified volumes as organ volumes approximates to zero. As a result, its precision values are much higher. However, because the previous method [3] usually incorrectly marks those volumes that are not positive volumes as positive volumes, its Recall and DSC values are generally not good. It should be noted that we should evaluate the performance of the model by considering generally various performance indexes. On the other hand, our proposed method can obtain much higher Recall and DSC values than those the previous method [3] and Laplacian smoothing method. Combining the vision results in Fig. 8 and the quantitative results in Table 2, we can see that our proposed method is more efficient compared with the previous method [3] and Laplacian smoothing method.

Table 2: Accurate evaluation of the proposed method. Laplacian smoothing method can be developed by using the following equation: $\phi_t = \Delta\phi + \lambda(\psi - \phi)$. Note that as $\varepsilon \to +\infty$, our method will become the Laplacian smoothing method.

Case	Our proposed method			Previous method [3]			Laplacian smoothing method		
	Recall	Precision	DSC	Recall	Precision	DSC	Recall	Precision	DSC
Spleen	**0.91**	0.98	**0.86**	0.78	**0.99**	0.62	0.88	0.96	0.75
Kidney(R)	**0.92**	0.98	**0.87**	0.76	**0.99**	0.64	0.87	0.96	0.82
Kidney(L)	**0.89**	**0.99**	**0.81**	0.78	**0.99**	0.64	0.83	0.97	0.75
Liver	**0.94**	0.96	**0.96**	0.89	**0.98**	0.81	0.89	0.94	0.90
Aorta	**0.93**	0.97	**0.91**	0.79	**0.99**	0.67	0.85	0.93	0.84

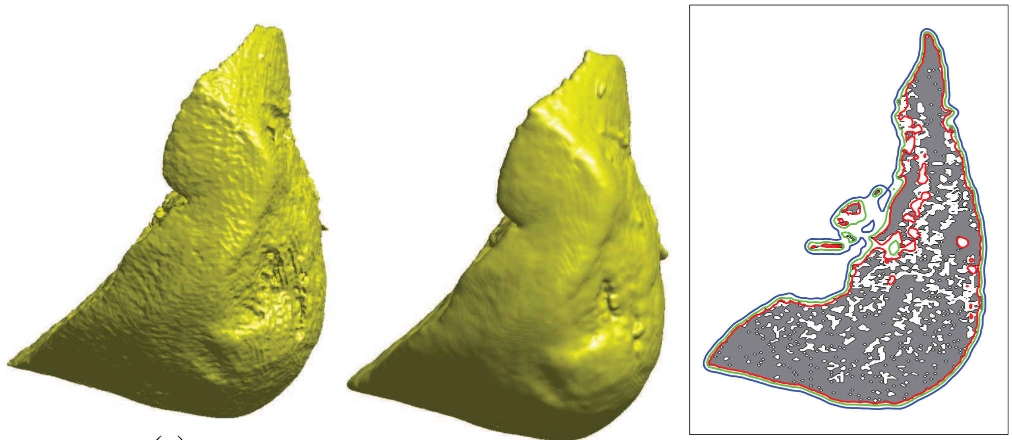

(a) (b) (c)

Figure 11: (a) 0.9 level of repaired volume, (b) 0.1 level of repaired volume, (c) show the cut view of repaired volume. To compared with the original volume, we put them together. Gray regions represent the original volume. Red, green, and blue lines denote 0.9, 0.5, and 0.1 levels of repaired volume, respectively.

4.2. Results with different levels of ϕ

Our proposed method has a merit that it can straightforwardly obtain the different probability distributions from the known volume $\psi(\mathbf{x})$. Figure 11 (a) and (b) show 0.9 and 0.1 levels of repaired volume (isosurface) from the original volume $\psi(\mathbf{x})$, respectively. These isosurfaces can be considered as the volumes, which have the 90% and 10% probabilities of repaired volume, respectively. Figure 11 (c) shows the cut view of repaired volume. To compare with the original volume, we put them together. Gray regions represent the original volume. Red, green, and blue lines denote 0.9, 0.5, and 0.1 levels of repaired volume, respectively. As can be seen, 0.9 level of ϕ is in good agreement with the real volume, which implies our model can remain the topology of volume. And other levels of repaired volume can provide the volume rendering information for users.

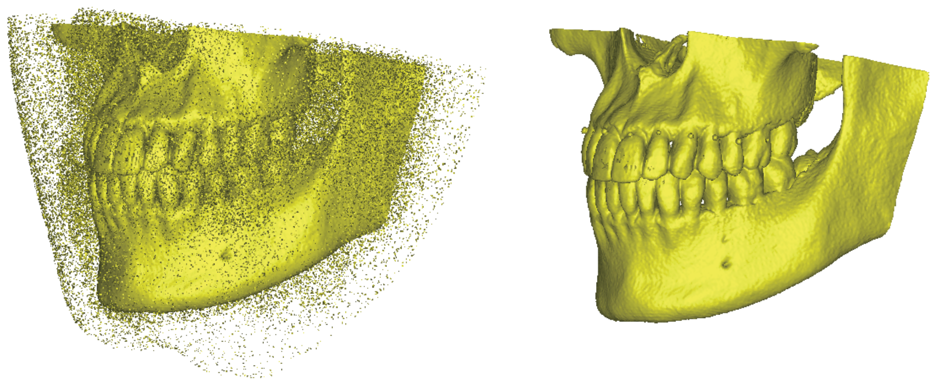

Figure 12: Volume repairing in removal of noises. From left to right, they are the known volume and repaired volume, respectively.

4.3. Removing noise points in the repairing

In practice, there are outliers or conflicting points in a given volume. Our proposed method can obtain a smooth volume, due to the mean curvature motion of Allen-Cahn equation. Figure 12 shows the volume repairing in removal of noises. From left to right, they are the given volume and repaired volume, respectively. As can be observed, our proposed method can obtain a clear result.

4.4. Parameter sensitivity analysis

In this section, we will perform parameter sensitivity analysis for the model parameters λ_0 and ε. The last term in Eq.(2) is the fidelity term that enforces new version (ϕ) to be the known volume (ψ). λ_0 balances the motion by the mean curvature flow and the fidelity term. If $\lambda_0 = 0$, our proposed method in Eq. (2) becomes the classical Allen-Cahn equation. With the classical Allen-Cahn equation, the noises are perfectly removed with missing the detail information of Aneurism as shown in Fig. 13(a). On the other hand, with a suitable large λ_0, our method (Eq. (2)) smooths away noises while preserving volume detail and sharp features as shown in Fig. 13(b). If the original volume is with high noises (10% Salt-and-pepper noise), λ_0 should be small to make the motion by the mean curvature flow be dominant. Thus the noises from the original volume can be removed (see Fig. 13(c)). Otherwise the fitting term is dominant and the restored volume tends to become the original one with noises (see Fig. 13(d)).

λ_0 is an importance parameter. However, how to choose a suitable value λ_0 is a question. Our proposed method can straightforwardly show the restriction of used λ_0. Observing Eq.(12), we can find that if λ_0 is larger than $10/\Delta t$, then $e^{-\lambda_0 \Delta t} \approx 0$ and $\check{\phi}^{n+1} \approx \psi$ for any time, which implies that the noise will remain (see Fig. 13(d)). We also can find that if $\lambda_0 < 0.1/\Delta t$, then $\phi^{n+1} \approx 0.9\phi^n + 0.1\psi$ will be much different with ψ. In this case, the results obtained by our proposed method will not be able to hold the original topological shape (see Fig. 13(a)). Therefore, we suggest to use $0.1/\Delta t < \lambda_0 < 10/\Delta t$. The role of ε is interface thickness of a

(a) (b) (c) (d)

Figure 13: Parameter sensitivity analysis for λ_0. From left to right, the first two results are repaired volumes for the volume without noises. The second two ones are for the volume with 10% Salt-and-pepper noises. (a) $\lambda_0 = 0$, (b) $\lambda_0 = 5$, (c) $\lambda_0 = 0.5$, and (d) $\lambda_0 = 5$.

transition layer of the separated region which represents two different states. We take the same initial condition except for different interface parameter values ε_5 and ε_{20}. From the results shown in Fig. 14, we can observe that when ε is too small, interfacial transition is too sharp. On the other hand, if it is too large, the volume will become thicker. It should be noted that we can see from Fig. 14 that whenever ε is larger or smaller used, our model can fill the small holes and remain the topology of the known volume.

Eqs. (2)-(4) keep the total energy $\mathscr{E}(\phi)$ decrease with time, which implies the solution of our proposed method is uniqueness. Therefore, we can stop the

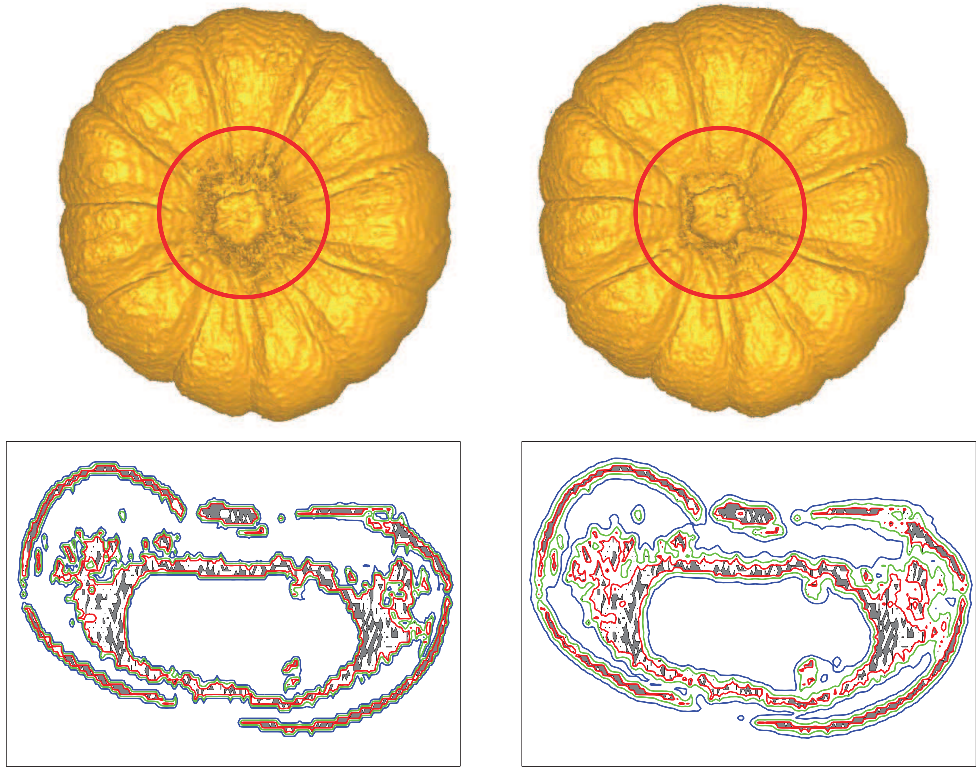

(a) (b)

Figure 14: Parameter sensitivity analysis for ε. (a) $\varepsilon = \varepsilon_5$, (b) $\varepsilon = \varepsilon_{20}$. Top row: whole view of repairing volume. Bottom row: vertical section of repaired volume. Gray regions represent the known volume. Red, green, and blue lines denote 0.9, 0.5, and 0.1 levels of repaired volume, respectively. When ε is too small, interfacial transition is too sharp. On the other hand, if is too large, the volume of volume will become thicker (See the circle region).

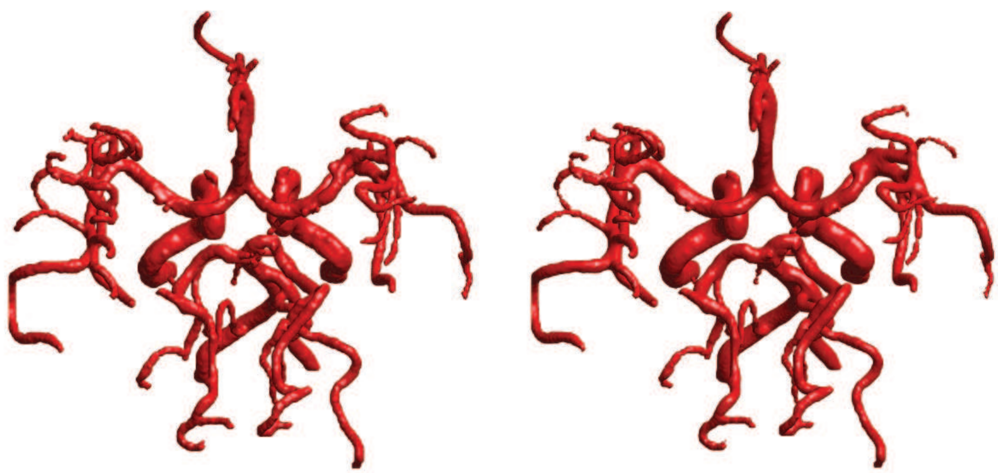

(a) (b)

Figure 15: Parameter sensitivity analysis for the stop condition. (a) $tol = 1e-2$. (b) $tol = 1e-6$.

evolution and regard the numerical result as the steady state solution, when the relative error $\|\phi^{n+1} - \phi^n\|_2^2 / \|\phi^n\|_2^2$ is less than a tolerance tol. Figure 15(a) and (b) show the repaired volume with $tol = 1e-2$ and $tol = 1e-6$, respectively. The used iterations are 6 and 98 for $tol = 1e-2$ and $tol = 1e-6$, respectively. As can be seen, the two results are much similar. Although the volume obtained by using $tol = 1e-6$ seems slightly smooth than that using $tol = 1e-2$, a larger tol requires much more iterations, until the relative error for the numerical solution is less than the given tol. The good stopping condition is important for the efficiency of our PDE based method. In this paper, we suggest to use $tol = 1e-4$.

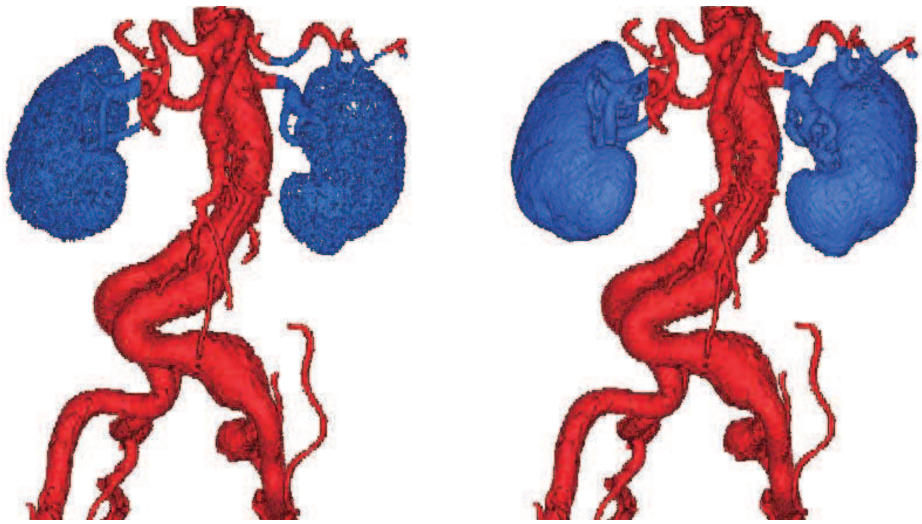

Figure 16: Repair defects over a specific patch. From left to right, they are initial volume and repaired volume, respectively. Here the blue region is the marked region.

4.5. Repair defects over a specific patch

In practice, we may want to repair defects over a specifically marked patch of the visualized volume but not over the whole visualized ψ. As shown in the left figure of Fig. 16, we only want to repair the Kidney over a specific patch which is marked as blue region, but not over the whole domain, because other regions are smooth without holes. Here we will modify our method to repair defects over a specific patch of the visualized volume, which is particularly marked by users. Assume Ω_M be the marked domain, which contains specific patch of the visualized volume, we introduce a control function $g(\mathbf{x})$, which is defined as

$$g(\mathbf{x}) = \begin{cases} 1 & \text{if } \mathbf{x} \in \Omega_M, \\ 0 & \text{otherwise.} \end{cases} \tag{19}$$

Then the extension of our proposed model can be defined as

$$\frac{\partial \phi}{\partial t} = g\left(-\frac{F'(\phi)}{\varepsilon^2} + \Delta\phi + \lambda(\psi - \phi)\right). \tag{20}$$

Observing Eq. (20), we can find that if $\mathbf{x}$ locates in Ω_M, we will perform our proposed method to repair defect. Otherwise, there will be no computations, which replies that the information in that regions will remain. A numerical test for CT aneurism image is performed and the numerical result is shown in Fig. 16. As can be seen, the volume repairing is successfully done.

5. Conclusion and future work

In this paper, we discussed volume repairing problem to generate high quality rendering results. By the constrained diffusion, we can adaptively adjust opacities of the voxels around known volume voxels, and well recover lost volume voxels. Consequently, visualization quality of volumes can be greatly improved in the volume rendering. Our method can be addressed without increasing the dimensionality of the TF. It allows us to incorporate our method into other processing or transfer functions. One limitation of our present implementation is that, since our method begins with the labeled volume voxels and is performed without depending on the TF, we can recover other lost volume voxels and remove the noises from volume data. But our method may fail to remove noises for the incorrect labeled volume voxels, since we do not have the corresponding sampling volume voxels in the hole regions. In the future, we will repair the volume by combining the 3D image gray values $f(\mathbf{x})$ and the labeled volume data. In practice, multiple volumes with defects need to be volume rendered from a volumetric data. We will extern our binary method into multiple method in future.

Acknowledgment

Y.B. Li is supported by National Natural Science Foundation of China (No.11601416) and by the China Postdoctoral Science Foundation (No.2018M640968). B.H. Lu is supported by Shaanxi Provincial Science and Technology Planning Project(2017KTZD6-01) and by Dongguan University of Technology High-level Talents (Innovation Team) Research Project (KCYCXPT2016003). L. Wang was supported in part by National Natural Science Foundation of China (No.61375020, No.61572317).

Reference

[1] H. Pfister, B. Lorensen, C. Bajaj, G. Kindlmann, W. Schroeder, L.S. Avila, K. Martin, R. Machiraju, J. Lee, The transfer function bake-off, IEEE Computer Graphics & Applications, 21(3)(2001)16–22.

[2] L. Wang, X. Zhao, and A. Kaufman, Modified dendrogram of attribute space for multidimensional transfer function design, IEEE Trans. Visualization & Computer Graphics,18(1)(2012) 121–131.

[3] S. Lan, L. Wang, Y. Song, Y. Wang, L. Yao, K. Sun, B. Xia, Z. Xu, Improving separability of structures with similar attributes in 2D transfer function design, IEEE Trans. Visualization & Computer Graphics, 23(5)(2017)1546–1560.

[4] Y. Wang, W. Chen, J. Zhang, T. Dong, G. Shan, X. Chi, Efficient volume exploration using the gaussian mixture model, IEEE Trans. Visualization & Computer Graphics, 17(11)(2011)560–1573.

[5] S. Roy, P. Maji, Rough segmentation of coherent local intensity for bias induced 3-D MR brain images, Pattern Recognition, 97 (2020) 106997

[6] T. Ilmanen, Convergence of the Allen-Cahn equation to Brakke's motion by mean curvature, Journal of Differential Geometry, 38 (2) (1993) 417-461.

[7] P. Sereda, A. Vilanova, I. W. O. Serlie, F. A. Gerritsen, Visualization of volumes in volumetric data sets using LH histograms, IEEE Trans. Visualization & Computer Graphics, 12(2) (2006) 208–218.

[8] S. Shafii, S. E. Dillard, M. Hlawitschka, B. Hamann, The topological effects of smoothing, IEEE Trans. Visualization & Computer Graphics, 18(1)(2012) 160-172.

[9] J. S. Suri, K. Liu, S. Singh, S. N. Laxminarayan, X. Zeng, L. Reden, Shape recovery algorithms using level sets in 2D/3D medical imagery: a state of the art review, IEEE Trans. Information technology in Biomedicine, 6 (1) (2002) 8-28.

[10] L. Wang, P. Wang, L. Cheng, Y. Ma, S. Wu, Y. Wang, Z. Xu, Detection and reconstruction of an implicit volume surface by adaptively expanding a small surface patch in a 3D image, IEEE Trans. Visualization & Computer Graphics, 20 (11) (2014) 1490–1506.

[11] G.M. Nielson, On marching cubes, IEEE Trans. Visualization & Computer Graphics, 9(3)(2003) 283–297.

[12] Y. Li, D. Lee, C. Lee, J. Lee, S. Lee, J. Kim, S. Ahn, J. Kim, Surface embedding narrow volume reconstruction from unorganized points, Computer Vision and Image Understanding, 121 (2014) 100-107.

[13] P. Labatut, J.P. Pons, R. Keriven, Robust and efficient surface reconstruction from range data, Computer Graphics Forum, 28 (8)(2009)2275–2290.

[14] M. Attene, M. Campen, L. Kobbelt, Polygon mesh repairing: An application perspective, ACM Computing Surveys, 45(2) (2013) 1–33.

[15] J. Davis, S. R. Marschner, M. Garr, M. Levoy, Filling holes in complex surfaces using volumetric diffusion, In: Proceedings of First International Symposium on 3D Data Processing, Visualization and Transmission, (2002) 428–441.

[16] S. Lindholm, D. Jnsson, C. Hansen, A. Ynnerman, Boundary aware reconstruction of scalar fields, IEEE Trans. Visualization and Computer Graphics, 20 (12) (2014)2447–2455.

[17] G. Lathen, S. Lindholm, R. Lenz, A. Persson, M. Borga, Automatic Ttuning of spatially varying transfer functions for blood vessel visualization, IEEE Trans. Visualization & Computer Graphics, 18 (12) (2012) 2345-2354.

[18] M. Janaszewski, M. Couprie, L. Babout, Hole fillingin 3D volumetric objects, Pattern Recognition,43 (2010) 3548–3559.

[19] Y. Li, H-G. Lee, D. Jeong, J. Kim, An unconditionally stable hybrid numerical method for solving the Allen–Cahn equation, Computers & Mathematics with Applications, 60(6) (2010) 1591–1606.

[20] Y. Li, J. Kim, Multiphase image segmentation using a phase-field model, Computers & Mathematics with Applications, 62(2) (2011): 737–745.

[21] Y. Li, D. Jeong, J-I. Choi, S. Lee, J. Kim, Fast local image inpainting based on the Allen-Cahn model, Digital Signal Processing, 37 (2015) 65–74.

[22] Y. Li, J. Kim, Fast and efficient narrow volume reconstruction from scattered data, Pattern Recognition, 48 (12) (2015) 4057–4069.

[23] Y. Li, J. Wang, B. Lu, D. Jeong, J. Kim, Multicomponent volume reconstruction from slice data using a modified multicomponent Cahn-Hilliard system, Pattern Recognition, 93 (2019) 124–133.

[24] R. Fedkiw, S. Osher, Level set methods and dynamic implicit surfaces, Springer, New York, 2002

[25] K. W. Morton, D. F. Mayers, Numerical solution of partial differential equations: An introduction, Cambridge University Press, 2005.